

CERN-EP/99-106

27 July 1999

Measurement of Inclusive $D^{*\pm}$ Production in Two-Photon Collisions at LEP

The L3 Collaboration

Abstract

Inclusive production of $D^{*\pm}$ mesons in two-photon collisions was measured by the L3 experiment at LEP. The data were collected at a centre-of-mass energy $\sqrt{s} = 189$ GeV with an integrated luminosity of 176.4 pb^{-1} . Differential cross sections of the process $e^+e^- \rightarrow e^+e^-D^{*\pm}X$ are determined as functions of the transverse momentum and pseudorapidity of the $D^{*\pm}$ mesons in the kinematic region $1 \text{ GeV} < p_T^{D^*} < 5 \text{ GeV}$ and $|\eta^{D^*}| < 1.4$. The cross section integrated over this phase space domain is measured to be $132 \pm 22(\text{stat.}) \pm 26(\text{syst.}) \text{ pb}$. The differential cross sections are compared with next-to-leading order perturbative QCD calculations.

Submitted to *Phys. Lett. B*

arXiv:hep-ex/9909005v1 3 Sep 1999

1 Introduction

The study of charm production in two-photon collisions provides a means for testing perturbative QCD and for probing the gluon content of the photon [1]. Charmed quarks can be produced in “direct-photon” processes, in which the interacting photons behave as point-like particles and couple directly to a charmed quark pair. Another class of processes contributing to the charm production are the “resolved-photon” processes, where one or both interacting photons fluctuate into a flux of partons. In the “single resolved-photon” processes the unresolved photon interacts with a constituent parton from the resolved photon, whereas in the “double resolved-photon” processes a hard scattering between the constituent partons of the two resolved photons takes place. In the next-to-leading order QCD only the sum of direct and resolved-photon processes is unambiguously defined. The experimental measurement of differential cross sections for production of open charmed particles allows a detailed investigation of the charm production mechanism.

Charm production in two-photon collisions has been measured at lower centre-of-mass energies at PEP, PETRA, TRISTAN and LEP [2–8], identifying charmed quarks by detecting $D^{*\pm}$ mesons, soft pions, inclusive leptons and K_S^0 mesons. In a previous measurement by the L3 experiment [9], events containing charmed quarks were tagged by detecting electrons and muons from semileptonic decays of charmed hadrons. In the present study charmed vector mesons $D^*(2010)^\pm$ are identified by the small energy released in D^* decay, applying the mass difference technique [10] to the decay chains ¹⁾

$$D^{*+} \rightarrow D^0 \pi_S^+ \begin{array}{l} \longleftarrow \\ \longrightarrow \end{array} K^- \pi^+ \quad (1)$$

$$\begin{array}{l} \longleftarrow \\ \longrightarrow \end{array} K^- \pi^+ \pi^0 \quad (2)$$

The presence of a low-momentum, “soft” pion, π_S^+ , ensures that the resolution of the mass difference $M(D^0 \pi_S^+) - M(D^0)$ is superior to the resolution of the reconstructed D^0 and D^{*+} masses themselves. The D^{*+} signal appears as a narrow peak close to the kinematic threshold in the mass difference distributions $M(K^- \pi^+ \pi_S^+) - M(K^- \pi^+)$ and $M(K^- \pi^+ \pi^0 \pi_S^+) - M(K^- \pi^+ \pi^0)$. The combined branching fractions are $\text{BR}(D^{*+} \rightarrow D^0 \pi_S^+) \cdot \text{BR}(D^0 \rightarrow K^- \pi^+) = 0.0263 \pm 0.0008$ and $\text{BR}(D^{*+} \rightarrow D^0 \pi_S^+) \cdot \text{BR}(D^0 \rightarrow K^- \pi^+ \pi^0) = 0.0949 \pm 0.0064$, as given in Reference [11].

2 Selection of Hadronic Two-Photon Events

The data were collected by the L3 detector [12] at LEP in 1998 at a centre-of-mass energy $\sqrt{s} = 189$ GeV. The integrated luminosity is 176.4 pb⁻¹.

For efficiency studies, samples of $e^+e^- \rightarrow e^+e^- \gamma^* \gamma^* \rightarrow e^+e^- c\bar{c}X$ events are generated using the PYTHIA [13] and the JAMVG [14] Monte Carlo generators. The background sources are simulated by JAMVG ($e^+e^- \rightarrow e^+e^- \tau^+ \tau^-$), KORALZ [15] ($e^+e^- \rightarrow \tau^+ \tau^- (\gamma)$), KORALW [16] ($e^+e^- \rightarrow W^+ W^- \rightarrow f \bar{f}' f' \bar{f}$) and PYTHIA ($e^+e^- \rightarrow q \bar{q} (\gamma)$, $e^+e^- \rightarrow e^+e^- q \bar{q}$). The Monte Carlo events are processed in the same way as the data.

Reconstruction of the decay chains (1) and (2) requires a sample of events containing hadronic final states. Events of the type $e^+e^- \rightarrow e^+e^- \gamma^* \gamma^* \rightarrow e^+e^- \text{hadrons}$ are selected by

¹⁾ The charge conjugate reactions are included throughout the paper.

cuts on the energy measured in the electromagnetic and hadron calorimeters and using tracking information. To exclude annihilation events, the total visible energy must not exceed $0.4\sqrt{s}$, the energy deposited in the electromagnetic calorimeter must be less than 30 GeV and the energy in the hadron calorimeter less than 40 GeV. The transverse component of the missing momentum vector must be less than 10 GeV and the value of the event thrust must be smaller than 0.95. Events are required to have at least three charged particles reconstructed in the tracking chamber.

A total of 1253890 events pass the hadron selection cuts. The contamination from annihilation processes and two-photon production of tau pairs is less than 0.5%. The subsequent reconstruction, which forms D^{*+} candidates from three-prong decays with invariant mass exceeding 2 GeV, suppresses these background contributions to a negligible level.

The trigger efficiency for detecting two-photon hadronic final states is $(87\pm 3)\%$, determined from the data sample itself using a set of independent triggers.

3 Mass Reconstruction of D^{*+} Decays

The identification of D^{*+} mesons proceeds through two steps: selection of D^0 candidates, which are then combined with another track to form D^{*+} candidates.

Tracks are used for reconstruction of D^0 decays if they satisfy the following requirements:

- Transverse momentum greater than 150 MeV.
- At least 40 wire hits measured by the tracking chamber.
- Distance of closest approach to the event vertex smaller than 1 mm in the transverse plane.

A pair of tracks of opposite charge is required to pass the following criteria in order to be considered as a $K^-\pi^+$ system from a D^0 decay:

- The intersection point of the tracks in the transverse plane must be displaced by no more than 3 mm away from the event vertex.
- $P_K \cdot P_\pi > 2 \cdot 10^{-3}$, where P_K and P_π are the probabilities, calculated from the measured energy loss dE/dX of each track, for kaon and pion mass hypotheses of the corresponding tracks.

The selection of tracks and their combinations into neutral pairs is identical for the channels (1) and (2) in order to minimize the relative systematic error between the two decay modes.

To reconstruct D^0 decays in the $K^-\pi^+\pi^0$ decay mode, a neutral pion is added to the selected $K^-\pi^+$ system. Neutral pion candidates are formed by a pair of photons, identified as isolated clusters in the electromagnetic calorimeter, not matched with a charged track. Photons are accepted for π^0 reconstruction if they are detected in the barrel part of the electromagnetic calorimeter and their energies are greater than 100 MeV. The π^0 candidates must have the invariant mass of the photon pair in the mass window of ± 15 MeV around the π^0 mass. The decay $D^0 \rightarrow K^-\pi^+\pi^0$ proceeds dominantly through one of the quasi-two-body intermediate states $\bar{K}^{*0}\pi^0$, $K^{*-}\pi^+$ and $K^-\rho^+$ [11]. We require either the invariant mass of a $K\pi$ subsystem to be within ± 80 MeV of the corresponding $K^*(892)$ mass or the invariant mass of the $\pi^+\pi^0$

system to be within ± 150 MeV of the ρ^+ mass. If this condition is met for a given intermediate resonant state, we make use of the P-wave properties of a vector particle decay into two scalar particles and demand in addition the helicity angle θ^* of the corresponding decay cascade to satisfy the condition $|\cos \theta^*| > 0.4$. The helicity angle θ^* is defined as the angle between the direction of a decay product of the vector resonance (\bar{K}^{*0} , K^{*-} or ρ^+) and the direction of the pseudoscalar particle (π^0 , π^+ or K^-) from the D^0 decay, calculated in the intermediate resonance rest frame.

To reduce the combinatorial background when reconstructing D^0 decays into the $K^-\pi^+$ final state, the opening angle of the track pair in space must be smaller than 2.5 rad. The combinatorial background for the $K^-\pi^+\pi^0$ decay mode is suppressed by requiring the solid angle, defined by the directions of flight of the three decay products, to be smaller than 2 sr.

The invariant mass of the $K^-\pi^+$ system is calculated and if it is in the range of ± 100 MeV around the mass of the D^0 mesons [11], the combination is retained as a D^0 candidate for the decay channel (1). The corresponding mass window for candidates in channel (2) is ± 50 MeV. The different mass windows reflect the corresponding D^0 mass resolutions, as obtained by Monte Carlo studies. The better resolution of the D^0 reconstruction in channel (2) is due to the softer and thus better measured charged particles produced in the three body decay and to the use of a well-measured π^0 .

Finally, the probability that a particular $K^-\pi^+$ combination comes from a D^0 decay in channel (1) is determined from a 1C kinematic fit, in which the invariant mass of the pair is constrained to the D^0 mass. For the $K^-\pi^+\pi^0$ final state we perform a 2C fit, constraining the mass of the whole system to the D^0 mass and the two-photon mass to the π^0 mass. A combination is accepted as a D^0 candidate if the confidence level of the fit is greater than 0.5%.

In the second step of the D^{*+} reconstruction, we consider all combinations of a given D^0 candidate with an additional track of positive charge, assumed to be the soft pion π_S^+ , resulting from the D^{*+} decay. A track used as a soft pion candidate must have a transverse momentum greater than 50 MeV, at least 25 wire hits measured by the tracking chamber, and a distance of closest approach to the event vertex smaller than 3 mm in the transverse plane.

A cut on the transverse momentum of the $D^0\pi_S^+$ system, $p_T > 1$ GeV, is imposed in order to exclude the region of small acceptance of D^{*+} .

The mass difference distribution $\Delta M = M(D^0\pi_S^+) - M(D^0)$ for the selected $D^0\pi_S^+$ combinations in the two channels is shown in Figure 1. The contributions from the decay cascades (1) and (2) accumulate in narrow peaks close to the kinematic threshold. The mass difference spectrum is fitted by a sum of a Gaussian function for the signal and a term for the background of the form $\sum_{i=1}^2 a_i(\Delta M - m_\pi)^{b_i}$, where a_i and b_i are free parameters. The peak positions, determined by the fit, are 145.5 ± 0.2 MeV for the channel (1) and 146.1 ± 0.3 MeV for the channel (2), and agree well with the world average value for the mass difference $m_{D^{*+}} - m_{D^0}$ [11]. The good description of the background by the fit is corroborated by a background estimate obtained from the data themselves employing an event-mixing technique. For this, D^0 candidates from a given event are combined with soft tracks from another event, containing D^0 candidates. The resulting background distributions are normalized to the data distributions in the region $\Delta M > 0.152$ GeV and shown in Figure 1 by the dashed histograms. The number of reconstructed $D^{*\pm}$ mesons is taken to be the number of observed entries in the signal region $0.141 \text{ GeV} < \Delta M < 0.150 \text{ GeV}$, less the integral of the background fit component over that region. The $D^{*\pm}$ signal is estimated to be 102 ± 17 events in channel (1) and 42 ± 11 in channel (2).

The combinatorial multiplicity in the signal regions $\Delta M < 0.150$ GeV is 1.04 ± 0.01 for the

channel (1) and 1.05 ± 0.02 for the channel (2). There is no overlap of events in this region between the two channels and since the corresponding peak positions of the $D^{*\pm}$ signal agree well, we add the two distributions shown in Figure 1 and the resulting mass difference spectrum is shown in Figure 2. The total number of the observed $D^{*\pm}$ mesons, obtained from the fit to the combined spectrum, is 149 ± 20 . If the combined spectrum is split into two distributions for negative and positive charmed events, the fit result is 66 ± 14 D^{*-} mesons and 76 ± 15 D^{*+} mesons.

4 Inclusive $D^{*\pm}$ Production Cross Section

The cross section of inclusive $D^{*\pm}$ production (summed over D^{*-} and D^{*+}) is determined in the visible kinematic region of experimental acceptance, to avoid model-dependent extrapolation uncertainties. In the present analysis, the selection cuts and the available statistics allow to cover the following phase space domain of $D^{*\pm}$ pseudorapidity $|\eta^{D^*}|$ and transverse momentum $p_T^{D^*}$:

$$\begin{aligned} |\eta^{D^*}| &< 1.4 \\ 1 \text{ GeV} < p_T^{D^*} &< 5 \text{ GeV}. \end{aligned} \tag{3}$$

The differential spectra are obtained by fits to the mass difference distributions subdivided into three intervals of $p_T^{D^*}$ or $|\eta^{D^*}|$, the other variable being integrated over its kinematic region. Based on Monte Carlo studies, the resolution of the reconstructed $p_T^{D^*}$ is determined to be about 30 MeV and the resolution of $|\eta^{D^*}|$ about 0.008 units of pseudorapidity. Thus the smearing and the resulting event migration between adjacent bins in the spectra of the reconstructed $D^{*\pm}$ mesons is negligible.

The efficiencies for the reconstruction of $D^{*\pm}$ mesons are calculated separately for direct-photon processes and for single resolved-photon processes with Monte Carlo events generated by the PYTHIA program. A massive matrix element calculation with charmed quark mass value $m_c = 1.35$ GeV and the SaS1d parametrization of the parton distributions of the photon [17] was used for the generation of events. The reconstruction efficiencies are calculated as a ratio of the combined number of reconstructed $D^{*\pm}$ mesons in the two decay channels to the number of generated $D^{*\pm}$ mesons and are presented in Figure 3 as functions of $p_T^{D^*}$ and $|\eta^{D^*}|$. Evaluated in this way, the efficiencies take into account the corresponding branching fractions of the decay modes (1) and (2). The two sets of efficiencies are similar and agree within the errors. This implies that the relative proportion of direct and resolved-photon contributions to the charm production is not a major source of uncertainty in the determination of the $D^{*\pm}$ differential cross sections in the phase space region defined by (3). Equal contributions of both types of charm production processes in the kinematic region (3) are assumed for the calculation of the reconstruction efficiencies, used for the cross-section evaluation.

The measured cross sections of inclusive $D^{*\pm}$ production, calculated as functions of $p_T^{D^*}$ and $|\eta^{D^*}|$ and integrated over the corresponding bin, are listed in Table 1. When evaluating the differential cross sections, a correction based on the prediction of the combined Monte Carlo sample, used for the efficiency determination, is calculated such as to assign the differential cross sections to the centres of the corresponding bins. The values of this correction are found to be different from one only for the cross section set $d\sigma/dp_T^{D^*}$ in the region of high $p_T^{D^*}$. The differential cross sections as a function of $p_T^{D^*}$, obtained after applying the bin-centre correction,

are listed in Table 1. The differential cross sections assigned to the bin centres are plotted in Figure 4 and Figure 5.

$p_T^{D^*}$ [GeV]	$\Delta\sigma_{meas}$ [pb]	$d\sigma/dp_T^{D^*}$ [pb / GeV]	$ \eta^{D^*} $	$\Delta\sigma_{meas}$ [pb]
1 – 2	$92.9 \pm 22.2 \pm 16.7$	$92.9 \pm 22.2 \pm 16.7$	0.0 – 0.4	$34.1 \pm 8.4 \pm 5.3$
2 – 3	$30.1 \pm 8.4 \pm 6.1$	$28.0 \pm 7.8 \pm 5.7$	0.4 – 0.8	$47.5 \pm 11.0 \pm 9.6$
3 – 5	$11.3 \pm 3.9 \pm 3.0$	$4.9 \pm 1.7 \pm 1.3$	0.8 – 1.4	$40.8 \pm 15.8 \pm 12.2$

Table 1: Measured cross sections $\Delta\sigma_{meas}$ for inclusive $D^{*\pm}$ production, integrated over the corresponding bin. The third column of the table gives the differential cross sections as a function of $p_T^{D^*}$ after bin-centre correction. The first errors are statistical, the second systematic.

The systematic uncertainties on the measured cross sections are estimated by varying the selection of tracks and photons and by varying the cuts throughout the $D^{*\pm}$ reconstruction. The contribution of the selection procedure to the systematic errors is in the range 8% – 17% affecting mostly the low- $p_T^{D^*}$ region. The uncertainties in the $K^-\pi^+\pi^0$ channel are higher than in the $K^-\pi^+$ channel. The systematic uncertainties related to the background estimation are determined by using different forms for the background function in the mass difference fit and by changing the mass range of the fit and are found to vary from 5% to 10%. The $D^{*\pm}$ reconstruction efficiencies are calculated also using a Monte Carlo sample generated by the JAMVG program which involves only direct processes in charm production, as well as for PYTHIA generations of direct and resolved processes with varied charmed quark mass value. The observed variations of the reconstruction efficiencies are taken into account as well as the Monte Carlo statistics, resulting in systematic changes of 5% – 14%. The contributions of the various sources of systematic errors are added in quadrature.

The integrated cross section measured in the visible kinematic region is found to be

$$\sigma(e^+e^- \rightarrow e^+e^-D^{*\pm}X; 1 \text{ GeV} < p_T^{D^*} < 5 \text{ GeV}, |\eta^{D^*}| < 1.4) = 132 \pm 22 \pm 26 \text{ pb},$$

where the first error is statistical and the second systematic.

The integrated cross sections calculated separately for the $K^-\pi^+$ and $K^-\pi^+\pi^0$ channels, $\sigma = 124 \pm 24 \text{ pb}$ and $\sigma = 142 \pm 46 \text{ pb}$ respectively (the errors are statistical only), agree well. This justifies combining the signals observed in the two decay modes.

In Figure 4 and Figure 5 the differential cross sections are compared to next-to-leading order perturbative QCD computations, based on a massless approach in calculating the parton-level cross sections [18]. In this scheme the charmed quark is considered to be one of the active flavours inside the photon. Three different sets of parton density parameterizations of the photon have been used in the calculations: GS [19], AFG [20] and GRV-HO [21]. The renormalization scale, μ_R , and the factorization scale of the photon structure function, μ_F , have been taken as $\mu_R = \mu_F/2 = \sqrt{p_T^2 + m_c^2}$ with charmed quark mass value $m_c = 1.5 \text{ GeV}$ [18]. There is a reasonable agreement between the data and the calculations. With regard to the variations of the predictions in the region of low transverse momentum, we should notice the limited applicability of the massless approach for $p_T \approx m_c$ [22].

5 Summary

The inclusive production of $D^{*\pm}$ mesons in two-photon interactions at LEP is measured by reconstructing D^{*+} cascade decays involving D^0 decays into $K^-\pi^+$ and $K^-\pi^+\pi^0$ final states, as well as the charge conjugate decay chains. The integrated and differential cross sections of inclusive $D^{*\pm}$ production are determined in the kinematic region $1 \text{ GeV} < p_T^{D^*} < 5 \text{ GeV}$, $|\eta^{D^*}| < 1.4$ for which the acceptance is found to be insensitive to the relative mixture of direct and single resolved-photon processes. In this phase space domain the integrated cross section is measured to be $\sigma(e^+e^- \rightarrow e^+e^-D^{*\pm}X) = 132 \pm 22(stat.) \pm 26(syst.) \text{ pb}$. A reasonable agreement is observed between the measured differential cross sections and the predictions based on next-to-leading order perturbative QCD calculations.

Acknowledgments

We express our gratitude to the CERN accelerator divisions for the excellent performance of the LEP machine. We also acknowledge and appreciate the effort of the engineers, technicians and support staff who have participated in the construction and maintenance of this experiment. We thank B.A. Kniehl for providing us with the results of QCD cross section calculations.

References

- [1] M. Drees, M. Krämer, J. Zunft and P.M. Zerwas, Phys. Lett. B **306** (1993) 371.
- [2] JADE Collab., W. Bartel *et al.*, Phys. Lett. B **184** (1987) 288.
- [3] TPC/Two-Gamma Collab., M. Alston-Garnjost *et al.*, Phys. Lett. B **252** (1990) 499.
- [4] TASSO Collab., W. Braunschweig *et al.*, Z. Phys. C **47** (1990) 499.
- [5] TOPAZ Collab., R. Enomoto *et al.*, Phys. Lett. B **328** (1994) 535; Phys. Rev. D **50** (1994) 1879; Phys. Lett. B **341** (1994) 238; M. Iwasaki *et al.*, Phys. Lett. B **341** (1994) 99.
- [6] VENUS Collab., S. Uehara *et al.*, Z. Phys. C **63** (1994) 213.
- [7] AMY Collab., T. Aso *et al.*, Phys. Lett. B **363** (1995) 249; N. Takashimizu *et al.*, Phys. Lett. B **381** (1996) 372.
- [8] ALEPH Collab., D. Buskulic *et al.*, Phys. Lett. B **355** (1995) 595.
- [9] L3 Collab., M. Acciarri *et al.*, Phys. Lett. B **453** (1999) 83.
- [10] S. Nussinov, Phys. Rev. Lett. **35** (1975) 1672; G.J. Feldman *et al.*, Phys. Rev. Lett. **38** (1977) 1313.
- [11] Particle Data Group, C. Caso *et al.*, Eur. Phys. J. C **3** (1998) 34.
- [12] L3 Collab., B. Adeva *et al.*, Nucl. Inst. Meth. **A 289** (1990) 35; M. Acciarri *et al.*, Nucl. Inst. Meth. **A 351** (1994) 300; M. Chemarin *et al.*, Nucl. Inst. Meth. **A 349** (1994) 345; I.C. Brock *et al.*, Nucl. Inst. Meth. **A 381** (1996) 236; A. Adam *et al.*, Nucl. Inst. Meth. **A 383** (1996) 342.
- [13] T. Sjöstrand, CERN-TH/7112/93 (1993), revised August 1995; T. Sjöstrand, Comp. Phys. Comm. **82** (1994) 74.
- [14] J.A.M. Vermaseren, Nucl. Phys. B **229** (1983) 347.
- [15] S. Jadach, B.F.L. Ward and Z. Was, Comp. Phys. Comm. **79** (1994) 503.
- [16] M. Skrzypek *et al.*, Comp. Phys. Comm. **94** (1996) 216; M. Skrzypek *et al.*, Phys. Lett. B **372** (1996) 289.
- [17] G.A. Schuler and T. Sjöstrand, Z. Phys. C **68** (1995) 607; Phys. Lett. B **376** (1996) 193.
- [18] J. Binnewies, B.A. Kniehl and G. Kramer, Phys. Rev. D **53** (1996) 6110; J. Binnewies, B.A. Kniehl and G. Kramer, Phys. Rev. D **58** (1998) 014014; B.A. Kniehl, private communication.
- [19] L.E. Gordon and J.K. Storrow, Nucl. Phys. B **489** (1997) 405.
- [20] P. Aurenche, J.-P. Guillet and M. Fontannaz, Z. Phys. C **64** (1994) 621.
- [21] M. Glück, E. Reya and A. Vogt, Phys. Rev. D **46** (1992) 1973.
- [22] S. Frixione *et al.*, Phys. Lett. B **319** (1993) 339.

The L3 Collaboration:

M.Acciarri,²⁶ P.Achard,¹⁹ O.Adriani,¹⁶ M.Aguilar-Benitez,²⁵ J.Alcaraz,²⁵ G.Alemanni,²² J.Allaby,¹⁷ A.Aloisio,²⁸ M.G.Alvigi,²⁸ G.Ambrosi,¹⁹ H.Anderhub,⁴⁷ V.P.Andreev,^{6,36} T.Angelescu,¹² F.Anselmo,⁹ A.Arefiev,²⁷ T.Azmoon,³ T.Aziz,¹⁰ P.Bagnaia,³⁵ L.Baksay,⁴² A.Balandras,⁴ R.C.Ball,³ S.Banerjee,¹⁰ Sw.Banerjee,¹⁰ A.Barczyk,^{47,45} R.Barillère,¹⁷ L.Barone,³⁵ P.Bartalini,²² M.Basile,⁹ R.Battiston,³² A.Bay,²² F.Becattini,¹⁶ U.Becker,¹⁴ F.Behner,⁴⁷ L.Bellucci,¹⁶ J.Berdugo,²⁵ P.Berges,¹⁴ B.Bertucci,³² B.L.Betev,⁴⁷ S.Bhattacharya,¹⁰ M.Biasini,³² A.Biland,⁴⁷ J.J.Blaising,⁴ S.C.Blyth,³³ G.J.Bobbink,² A.Böhm,¹ L.Boldizar,¹³ B.Borgia,³⁵ D.Bourilkov,⁴⁷ M.Bourquin,¹⁹ S.Braccini,¹⁹ J.G.Branson,³⁸ V.Brigljevic,⁴⁷ F.Brochu,⁴ A.Buffini,¹⁶ A.Buijs,⁴³ J.D.Burger,¹⁴ W.J.Burger,³² J.Busenitz,⁴² A.Button,³ X.D.Cai,⁴ M.Campanelli,⁴⁷ M.Capell,¹⁴ G.Cara Romeo,⁹ G.Carlino,²⁸ A.M.Cartacci,¹⁶ J.Casaus,²⁵ G.Castellini,¹⁶ F.Cavallari,³⁵ N.Cavallo,²⁸ C.Cecchi,¹⁹ M.Cerrada,²⁵ F.Cesaroni,²³ M.Chamizo,¹⁹ Y.H.Chang,⁴⁹ U.K.Chaturvedi,¹⁸ M.Chemarin,²⁴ A.Chen,⁴⁹ G.Chen,⁷ G.M.Chen,⁷ H.F.Chen,²⁰ H.S.Chen,⁷ X.Chereau,⁴ G.Chiefari,²⁸ L.Cifarelli,³⁷ F.Cindolo,⁹ C.Civinini,¹⁶ I.Clare,¹⁴ R.Clare,¹⁴ G.Coignet,⁴ A.P.Colijn,² N.Colino,²⁵ S.Costantini,⁸ F.Cotorobai,¹² B.Cozzoni,⁹ B.de la Cruz,²⁵ A.Csilling,¹³ S.Cucciarelli,³² T.S.Dai,¹⁴ J.A.van Dalen,³⁰ R.D'Alessandro,¹⁶ R.de Asmundis,²⁸ P.Déglon,¹⁹ A.Degré,⁴ K.Deiters,⁴⁵ D.della Volpe,²⁸ P.Denes,³⁴ F.DeNotaristefani,³⁵ A.De Salvo,⁴⁷ M.Diemoz,³⁵ D.van Dierendonck,² F.Di Lodovico,⁴⁷ C.Dionisi,³⁵ M.Dittmar,⁴⁷ A.Dominguez,³⁸ A.Doria,²⁸ M.T.Dova,^{18,†} D.Duchesneau,⁴ D.Dufournand,⁴ P.Duinker,² I.Duran,³⁹ H.El Mamouni,²⁴ A.Engler,³³ F.J.Eppling,¹⁴ F.C.Erné,² P.Extermann,¹⁹ M.Fabre,⁴⁵ R.Faccini,³⁵ M.A.Falagan,²⁵ S.Falciano,^{35,17} A.Favara,¹⁷ J.Fay,²⁴ O.Fedin,³⁶ M.Felcini,⁴⁷ T.Ferguson,³³ F.Ferroni,³⁵ H.Fesefeldt,¹ E.Fiandrini,³² J.H.Field,¹⁹ F.Filthaut,¹⁷ P.H.Fisher,¹⁴ I.Fisk,³⁸ G.Forconi,¹⁴ L.Fredj,¹⁹ K.Freudenreich,⁴⁷ C.Furetta,²⁶ Yu.Galaktionov,^{27,14} S.N.Ganguli,¹⁰ P.Garcia-Abia,⁵ M.Gataullin,³¹ S.S.Gau,¹¹ S.Gentile,^{35,17} N.Gheordanescu,¹² S.Giagu,³⁵ Z.F.Gong,²⁰ G.Grenier,²⁴ O.Grimm,⁸ M.W.Gruenewald,⁸ M.Guida,³⁷ R.van Gulik,² V.K.Gupta,³⁴ A.Gurtu,¹⁰ L.J.Gutay,⁴⁴ D.Haas,⁵ A.Hasan,²⁹ D.Hatzifotiadou,⁸ T.Hebbeker,⁸ A.Herve,¹⁷ P.Hidas,¹³ J.Hirschfelder,³³ H.Hofer,⁴⁷ G.Holzner,⁴⁷ H.Hoorani,³³ S.R.Hou,⁴⁹ I.Iashvili,⁴⁶ B.N.Jin,⁷ L.W.Jones,³ P.de Jong,² I.Josa-Mutuberría,²⁵ R.A.Khan,¹⁸ D.Kamrad,⁴⁶ M.Kaur,^{18,◇} M.N.Kienzle-Focacci,¹⁹ D.Kim,³⁵ D.H.Kim,⁴¹ J.K.Kim,⁴¹ S.C.Kim,⁴¹ J.Kirkby,¹⁷ D.Kiss,¹³ W.Kittel,³⁰ A.Klimentov,^{14,27} A.C.König,³⁰ A.Kopp,⁴⁶ I.Korolok,²⁷ V.Koutsenko,^{14,27} M.Kräber,⁴⁷ R.W.Kraemer,³³ W.Krenz,¹ A.Kunin,^{14,27} P.Ladron de Guevara,²⁵ I.Laktineh,²⁴ G.Landi,¹⁶ K.Lassila-Perini,⁴⁷ P.Laurikainen,²¹ A.Lavorato,³⁷ M.Lebeau,¹⁷ A.Lebedev,¹⁴ P.Lebun,²⁴ P.Lecomte,⁴⁷ P.Lecoq,¹⁷ P.Le Coultre,⁴⁷ H.J.Lee,⁸ J.M.Le Goff,¹⁷ R.Leiste,⁴⁶ E.Leonardi,³⁵ P.Levtchenko,³⁶ C.Li,²⁰ C.H.Lin,⁴⁹ W.T.Lin,⁴⁹ F.L.Linde,² L.Lista,²⁸ Z.A.Liu,⁷ W.Lohmann,⁴⁶ E.Longo,³⁵ Y.S.Lu,⁷ K.Lübelsmeyer,¹ C.Luci,^{17,35} D.Luckey,¹⁴ L.Lugnier,²⁴ L.Luminari,³⁵ W.Lustermann,⁴⁷ W.G.Ma,²⁰ M.Maity,¹⁰ L.Malgeri,¹⁷ A.Malinin,^{27,17} C.Mañá,²⁵ D.Mangeol,³⁰ P.Marchesini,⁴⁷ G.Marian,¹⁵ J.P.Martin,²⁴ F.Marzano,³⁵ G.G.G.Massaró,² K.Mazumdar,¹⁰ R.R.McNeil,⁶ S.Mele,¹⁷ L.Merola,²⁸ M.Meschini,¹⁶ W.J.Metzger,³⁰ M.von der Mey,¹ A.Mihul,¹² H.Milcent,¹⁷ G.Mirabelli,³⁵ J.Mnich,¹⁷ G.B.Mohanty,¹⁰ P.Molnar,⁸ B.Monteoloni,^{16,†} T.Moulik,¹⁰ G.S.Muanza,²⁴ F.Muheim,¹⁹ A.J.M.Muijs,² M.Musy,³⁵ M.Napolitano,²⁸ F.Nessi-Tedaldi,⁴⁷ H.Newman,³¹ T.Niessen,¹ A.Nisati,³⁵ H.Nowak,⁴⁶ Y.D.Oh,⁴¹ G.Organtini,³⁵ R.Ostonen,²¹ C.Palomares,²⁵ D.Pandoulas,¹ S.Paoletti,^{35,17} P.Paolucci,²⁸ R.Paramatti,³⁵ H.K.Park,³³ I.H.Park,⁴¹ G.Pascale,³⁵ G.Passaleva,¹⁷ S.Patricelli,²⁸ T.Paul,¹¹ M.Pauluzzi,³² C.Paus,¹⁷ F.Pauss,⁴⁷ D.Peach,¹⁷ M.Pedace,³⁵ S.Pensotti,²⁶ D.Perret-Gallix,⁴ B.Petersen,³⁰ D.Piccolo,²⁸ F.Pierella,⁹ M.Pieri,¹⁶ P.A.Piroué,³⁴ E.Pistoletti,²⁶ V.Plyaskin,²⁷ M.Pohl,⁴⁷ V.Pojidaev,^{27,16} H.Postema,¹⁴ J.Pothier,¹⁷ N.Produit,¹⁹ D.O.Prokofiev,⁴⁴ D.Prokofiev,³⁶ J.Quartieri,³⁷ G.Rahal-Callot,^{47,17} M.A.Rahaman,¹⁰ P.Raics,¹⁵ N.Raja,¹⁰ R.Ramelli,⁴⁷ P.G.Rancoita,²⁶ G.Raven,³⁸ P.Razis,²⁹ D.Ren,⁴⁷ M.Rescigno,³⁵ S.Reucroft,¹¹ T.van Rhee,⁴³ S.Riemann,⁴⁶ K.Riles,³ A.ROBOHM,⁴⁷ J.Rodin,⁴² B.P.Roe,³ L.Romero,²⁵ A.Rosca,⁸ S.Rosier-Lees,⁴ J.A.Rubio,¹⁷ D.Ruschmeier,⁸ H.Rykaczewski,⁴⁷ S.Sarkar,³⁵ J.Salicio,¹⁷ E.Sanchez,¹⁷ M.P.Sanders,³⁰ M.E.Sarakinos,²¹ C.Schäfer,¹ V.Schegelsky,³⁶ S.Schmidt-Kaerst,¹ D.Schmitz,¹ H.Schopper,⁴⁸ D.J.Schotanus,³⁰ G.Schwering,¹ C.Sciacca,²⁸ D.Sciarrino,¹⁹ A.Seganti,⁹ L.Servoli,³² S.Shevchenko,³¹ N.Shivarov,⁴⁰ V.Shoutko,²⁷ E.Shumilov,²⁷ A.Shvorob,³¹ T.Siedenburg,¹ D.Son,⁴¹ B.Smith,³³ P.Spillantini,¹⁶ M.Steuer,¹⁴ D.P.Stickland,³⁴ A.Stone,⁶ H.Stone,^{34,†} B.Stoyanov,⁴⁰ A.Straessner,¹ K.Sudhakar,¹⁰ G.Sultanov,¹⁸ L.Z.Sun,²⁰ H.Suter,⁴⁷ J.D.Swain,¹⁸ Z.Szillasi,^{42,¶} T.Sztarichai,^{42,¶} X.W.Tang,⁷ L.Tauscher,⁵ L.Taylor,¹¹ C.Timmermans,³⁰ Samuel C.C.Ting,¹⁴ S.M.Ting,¹⁴ S.C.Tonwar,¹⁰ J.Tóth,¹³ C.Tully,³⁴ K.L.Tung,⁷ Y.Uchida,¹⁴ J.Ulbricht,⁴⁷ E.Valente,³⁵ G.Vesztegombi,¹³ I.Vetlitsky,²⁷ D.Vicinanza,³⁷ G.Viertel,⁴⁷ S.Villa,¹¹ M.Vivargent,⁴ S.Vlachos,⁵ I.Vodopianov,³⁶ H.Vogel,³³ H.Vogt,⁴⁶ I.Vorobiev,²⁷ A.A.Vorobyov,³⁶ A.Vorvolakos,²⁹ M.Wadhwa,⁵ W.Wallraff,¹ M.Wang,¹⁴ X.L.Wang,²⁰ Z.M.Wang,²⁰ A.Weber,¹ M.Weber,¹ P.Wienemann,¹ H.Wilkens,³⁰ S.X.Wu,¹⁴ S.Wynhoff,¹ L.Xia,³¹ Z.Z.Xu,²⁰ B.Z.Yang,²⁰ C.G.Yang,⁷ H.J.Yang,⁷ M.Yang,⁷ J.B.Ye,²⁰ S.C.Yeh,³⁰ An.Zalite,³⁶ Yu.Zalite,³⁶ Z.P.Zhang,²⁰ G.Y.Zhu,⁷ R.Y.Zhu,³¹ A.Zichichi,^{9,17,18} F.Ziegler,⁴⁶ G.Zilizi,^{42,¶} M.Zöller,¹

- 1 I. Physikalisches Institut, RWTH, D-52056 Aachen, FRG[§]
 - III. Physikalisches Institut, RWTH, D-52056 Aachen, FRG[§]
 - 2 National Institute for High Energy Physics, NIKHEF, and University of Amsterdam, NL-1009 DB Amsterdam, The Netherlands
 - 3 University of Michigan, Ann Arbor, MI 48109, USA
 - 4 Laboratoire d'Annecy-le-Vieux de Physique des Particules, LAPP, IN2P3-CNRS, BP 110, F-74941 Annecy-le-Vieux CEDEX, France
 - 5 Institute of Physics, University of Basel, CH-4056 Basel, Switzerland
 - 6 Louisiana State University, Baton Rouge, LA 70803, USA
 - 7 Institute of High Energy Physics, IHEP, 100039 Beijing, China[△]
 - 8 Humboldt University, D-10099 Berlin, FRG[§]
 - 9 University of Bologna and INFN-Sezione di Bologna, I-40126 Bologna, Italy
 - 10 Tata Institute of Fundamental Research, Bombay 400 005, India
 - 11 Northeastern University, Boston, MA 02115, USA
 - 12 Institute of Atomic Physics and University of Bucharest, R-76900 Bucharest, Romania
 - 13 Central Research Institute for Physics of the Hungarian Academy of Sciences, H-1525 Budapest 114, Hungary[‡]
 - 14 Massachusetts Institute of Technology, Cambridge, MA 02139, USA
 - 15 Lajos Kossuth University-ATOMKI, H-4010 Debrecen, Hungary[¶]
 - 16 INFN Sezione di Firenze and University of Florence, I-50125 Florence, Italy
 - 17 European Laboratory for Particle Physics, CERN, CH-1211 Geneva 23, Switzerland
 - 18 World Laboratory, FBLJA Project, CH-1211 Geneva 23, Switzerland
 - 19 University of Geneva, CH-1211 Geneva 4, Switzerland
 - 20 Chinese University of Science and Technology, USTC, Hefei, Anhui 230 029, China[△]
 - 21 SEFT, Research Institute for High Energy Physics, P.O. Box 9, SF-00014 Helsinki, Finland
 - 22 University of Lausanne, CH-1015 Lausanne, Switzerland
 - 23 INFN-Sezione di Lecce and Università Degli Studi di Lecce, I-73100 Lecce, Italy
 - 24 Institut de Physique Nucléaire de Lyon, IN2P3-CNRS, Université Claude Bernard, F-69622 Villeurbanne, France
 - 25 Centro de Investigaciones Energéticas, Medioambientales y Tecnológicas, CIEMAT, E-28040 Madrid, Spain^b
 - 26 INFN-Sezione di Milano, I-20133 Milan, Italy
 - 27 Institute of Theoretical and Experimental Physics, ITEP, Moscow, Russia
 - 28 INFN-Sezione di Napoli and University of Naples, I-80125 Naples, Italy
 - 29 Department of Natural Sciences, University of Cyprus, Nicosia, Cyprus
 - 30 University of Nijmegen and NIKHEF, NL-6525 ED Nijmegen, The Netherlands
 - 31 California Institute of Technology, Pasadena, CA 91125, USA
 - 32 INFN-Sezione di Perugia and Università Degli Studi di Perugia, I-06100 Perugia, Italy
 - 33 Carnegie Mellon University, Pittsburgh, PA 15213, USA
 - 34 Princeton University, Princeton, NJ 08544, USA
 - 35 INFN-Sezione di Roma and University of Rome, "La Sapienza", I-00185 Rome, Italy
 - 36 Nuclear Physics Institute, St. Petersburg, Russia
 - 37 University and INFN, Salerno, I-84100 Salerno, Italy
 - 38 University of California, San Diego, CA 92093, USA
 - 39 Dept. de Física de Partículas Elementales, Univ. de Santiago, E-15706 Santiago de Compostela, Spain
 - 40 Bulgarian Academy of Sciences, Central Lab. of Mechatronics and Instrumentation, BU-1113 Sofia, Bulgaria
 - 41 Center for High Energy Physics, Adv. Inst. of Sciences and Technology, 305-701 Taejeon, Republic of Korea
 - 42 University of Alabama, Tuscaloosa, AL 35486, USA
 - 43 Utrecht University and NIKHEF, NL-3584 CB Utrecht, The Netherlands
 - 44 Purdue University, West Lafayette, IN 47907, USA
 - 45 Paul Scherrer Institut, PSI, CH-5232 Villigen, Switzerland
 - 46 DESY, D-15738 Zeuthen, FRG
 - 47 Eidgenössische Technische Hochschule, ETH Zürich, CH-8093 Zürich, Switzerland
 - 48 University of Hamburg, D-22761 Hamburg, FRG
 - 49 National Central University, Chung-Li, Taiwan, China
 - 50 Department of Physics, National Tsing Hua University, Taiwan, China
- [§] Supported by the German Bundesministerium für Bildung, Wissenschaft, Forschung und Technologie
[‡] Supported by the Hungarian OTKA fund under contract numbers T019181, F023259 and T024011.
[¶] Also supported by the Hungarian OTKA fund under contract numbers T22238 and T026178.
^b Supported also by the Comisión Interministerial de Ciencia y Tecnología.
[‡] Also supported by CONICET and Universidad Nacional de La Plata, CC 67, 1900 La Plata, Argentina.
[△] Also supported by Panjab University, Chandigarh-160014, India.
[△] Supported by the National Natural Science Foundation of China.
[†] Deceased.

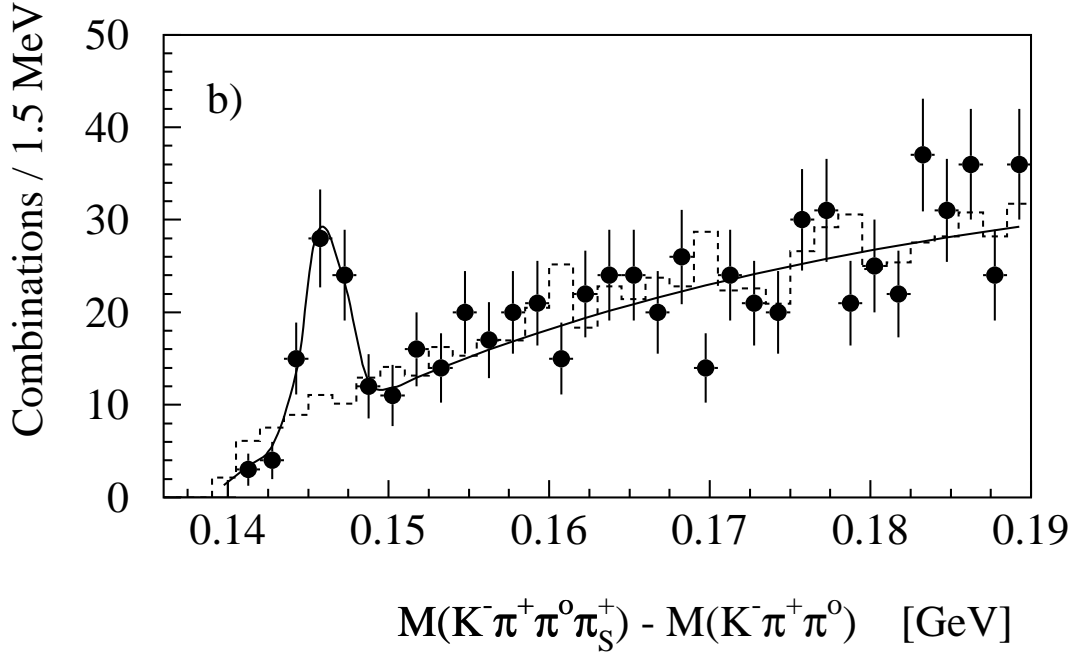
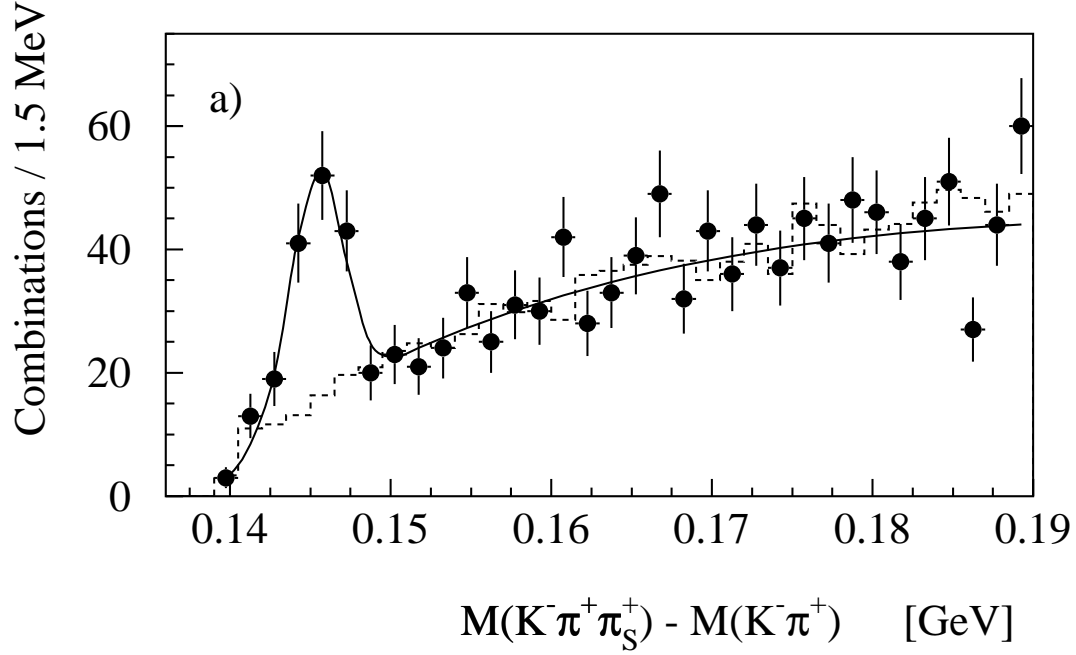


Figure 1: Mass difference distribution for D^0 decays into (a) $K^- \pi^+$ and (b) $K^- \pi^+ \pi^0$. The points are data, the line is the result of the fit to the data points used to evaluate the D^{*+} signal and the dashed histogram represents a background check, see the text.

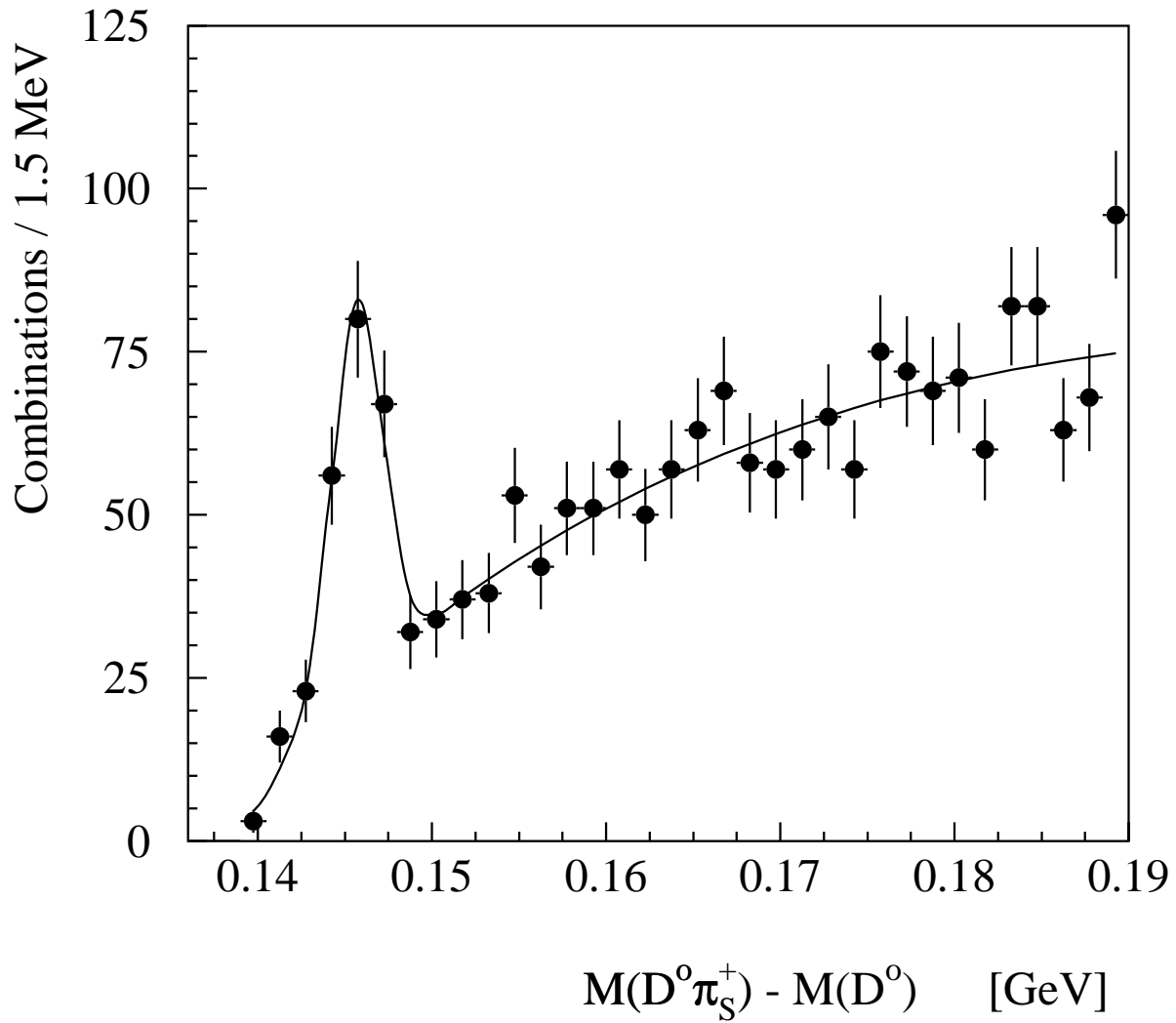


Figure 2: Combined mass difference distribution for D^0 decay channels $K^-\pi^+$ and $K^-\pi^+\pi^0$. The points are data and the line is the result of the fit used to evaluate the D^{*+} signal.

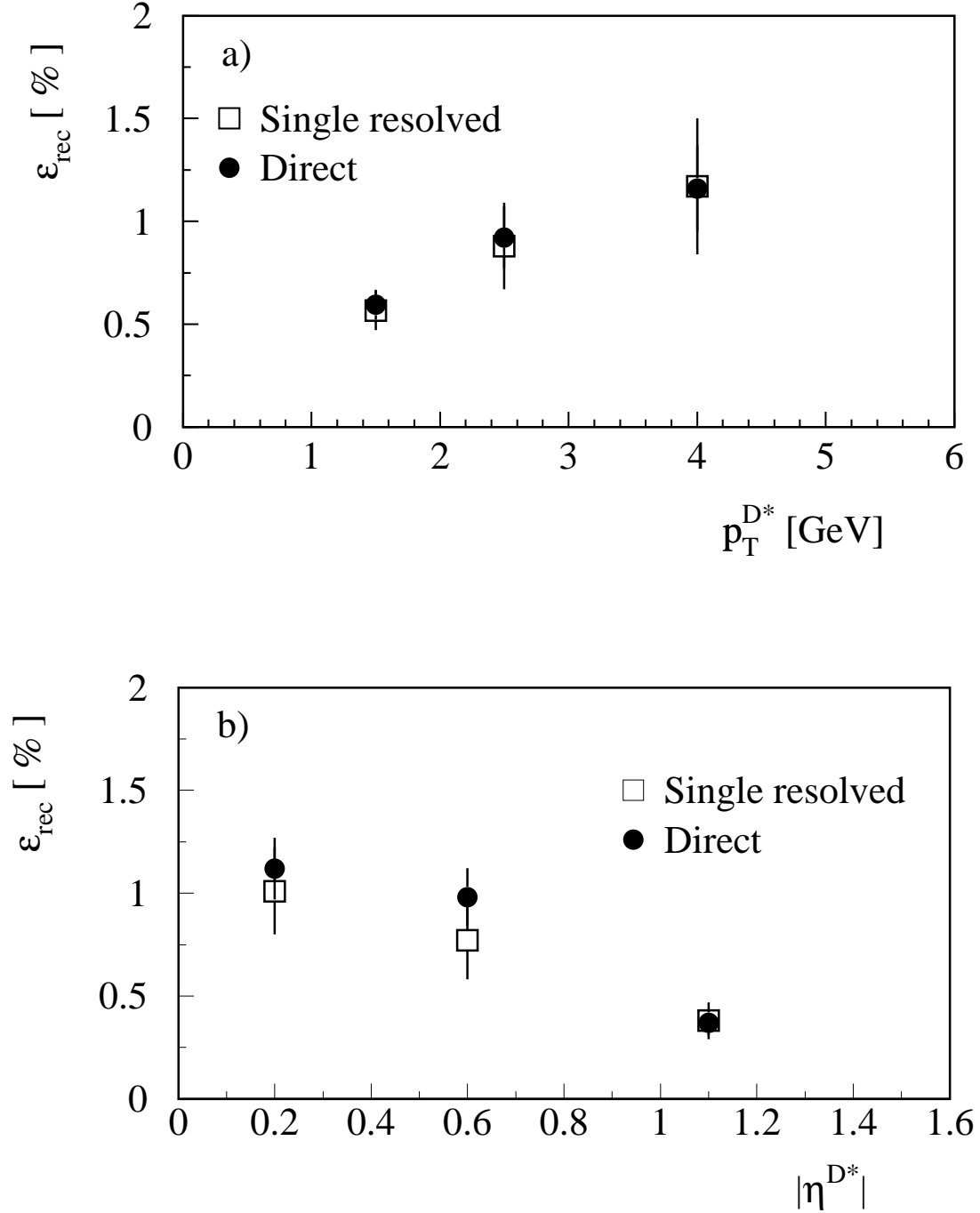


Figure 3: Reconstruction efficiency of $\text{D}^{*\pm}$ mesons (including the branching fractions), determined from PYTHIA generation of direct and single resolved-photon processes (a) as a function of $p_T^{\text{D}^*}$ for $|\eta^{\text{D}^*}| < 1.4$ and (b) as a function of $|\eta^{\text{D}^*}|$ for $1 \text{ GeV} < p_T^{\text{D}^*} < 5 \text{ GeV}$.

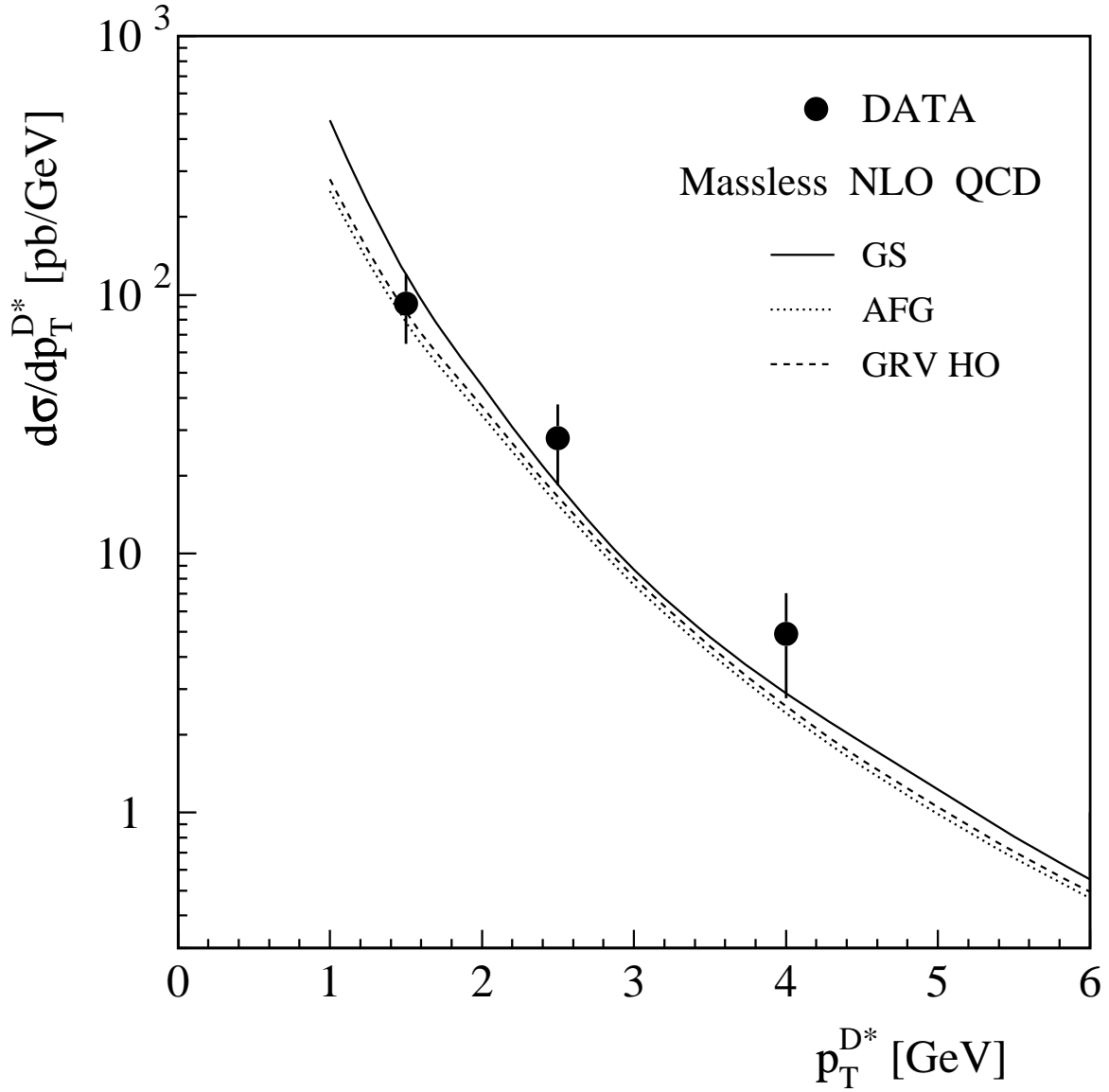


Figure 4: The differential cross section of $D^{*\pm}$ production as a function of the transverse momentum of the $D^{*\pm}$ mesons for $|\eta^{D^*}| < 1.4$. The points represent the data, the error bars show the statistical and systematic errors added in quadrature. The curves represent next-to-leading order QCD calculations [18] for different parameterizations of the parton densities of the photon (GS [19], AFG [20] and GRV-HO [21]).

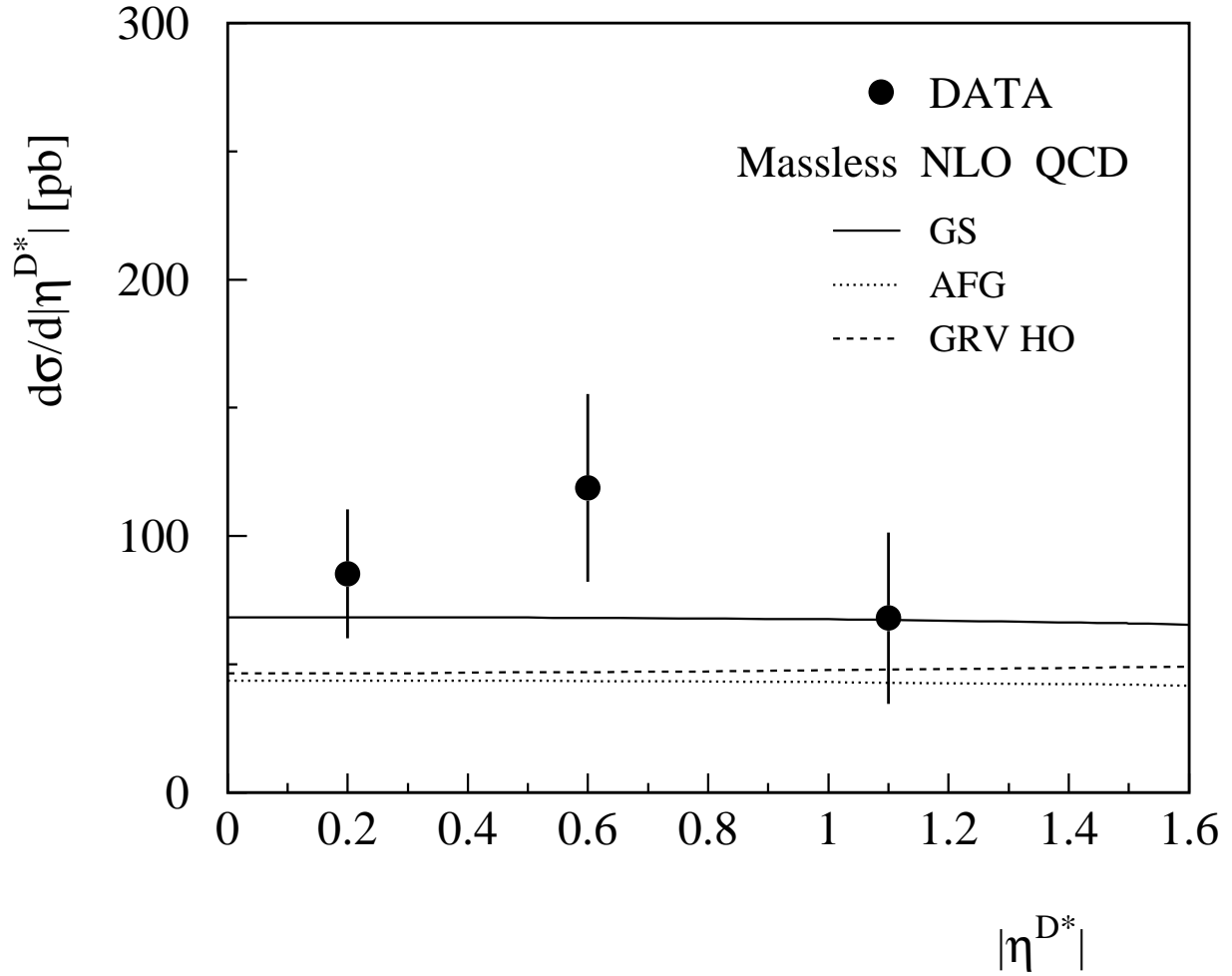


Figure 5: The differential cross section of $D^{*\pm}$ production as a function of the pseudorapidity of the $D^{*\pm}$ mesons for $1 \text{ GeV} < p_T^{D^*} < 5 \text{ GeV}$. The points represent the data, the error bars show the statistical and systematic errors added in quadrature. The curves represent next-to-leading order QCD calculations as in Figure 4.